Hydrogeochemical and Stable Isotope Processes of Groundwater in Laayoune-Dakhla (Southern Sahara, Morocco)

K. Mizeb[1], M. Doubi[1], M. Ghalit[2], M. El Kanti[1], H. Erramli[1] and R. Touir[3,4*]

[1]*Organic and Inorganic Chemistry, Electrochemistry and Environment Laboratory, Faculty of Sciences, Ibn Tofail University, Kenitra, Morocco*
[2]*Applied Chemistry and Environment Laboratory, Solid Mineral Chemistry Team, Faculty of Sciences, Mohammed First University, Oujda, Morocco*
[3]*Advanced Materials and Process Engineering Laboratory, Faculty of Sciences, Ibn Tofail university, Kenitra, Morocco*
[4]*Regional Centre for Education and Training Professions (CRMEF), Kenitra, Morocco*
*Corresponding author: touir8@gmail.com, touir8@yahoo.fr

Received 14/05/2023; accepted 20/07/2023
https://doi.org/10.4152/pea.2024420604

Abstract
In this study, to determine chemical elements and stable isotopes in 30 GW samples collected from SS Moroccan L-D region, various analytical techniques were used. Thus, the goal was to identify and understand different geochemical processes contributing to water mineralization in the study area. In fact, statistical results for major cations and anions indicated that they obeyed the following trend: $Na^+ > Ca^{2+} > Mg^{2+} > K^+$, and $Cl^- > SO_4^{2-} > HCO_3^- > NO_3^-$, respectively. Additionally, it was found that water EC values varied from 1290 to 6895 µs/cm. Indeed, pH values of investigated GW was from 6.88 to 7.75. Studied GW had HG facies with 86.66% Na-Cl and 13.33% Ca-SO_4. This finding is explained by the dissolution of evaporative formations that characterizes Saharan sections. Additionally, ionic ratios analysis revealed that GW chemical evolution was influenced by processes such as rock weathering, mineral compounds dissolution and evaporation. Therefore, a better relationship between Ca and SO_4 suggested gypsum and anhydrite leaching. It was found that stable isotopes ($\delta^{18}O$ and δ^2H) values differed from -6.96 to -8.93‰ and from -51.5 to 65.56‰, respectively. These findings strongly suggest that waters in the region undergo significant evaporation before reaching the aquifer. In addition, the aquifer's recharge height was also predicted to be no higher than 300 m, with a latitudinal gradient of $\delta^{18}O$, including 0.52 per 100 m. These results can serve as valuable guidance for decision makers in optimizing exploitation and assessment processes in Moroccan SS area.

Keywords: AAS; GW; HG; mineralization; Moroccan SS; stable isotopic.

Introduction•

GW is a valuable and essential natural resource, flowing in underground geological aquifers or onto the surface. Thus, its chemical composition is linked to the existing environment [1, 2]. Understanding HG is important to establish

• The abbreviations and symbols definition lists are in pages 448-449.

the source of GW chemical composition and its interaction with rocks [3]. It is also known that water quality is a significant factor influencing both human and animal health [4]. Likewise, natural processes and human activity affect water quality [5, 6]. Therefore, the knowledge of GW characteristics is vital for its management in the studied area [7]. Indeed, different ionic ratios can be employed to describe water chemical composition, like some researchers have done, to point out GW chemistry evolution [8-10].

Various investigations have discovered that several geochemical procedures, such as ion exchange, evaporation, rock weathering and mineral dissolution influence GW chemistry proprieties [11]. Then, whether water is for drinking or agriculture purposes depends on MW chemical composition; numerous investigators have examined surface water and GW hydrochemistry to assess if they are potable [12, 13].

However, GW in deep aquifers generally retains its stable isotopic signature ($\delta^{18}O$, $\delta^{2}H$) without being mixed with waters of different isotopic composition. Thus, stable isotopic configuration is used to distinguish fresh GW of isotopically separated bases from meteoric waters [14], such as vaporized water, during perpendicular transfer to unconfined or surface aquifers [15]. However, it is known that fresh water $\delta^{2}H/\delta^{18}O$ fraction differs, due to latitudinal and chronological climatic systems, which allow for precipitation waters dispersion throughout geographic areas [16]. In addition, this fraction strongly depends on T, altitude, latitude, precipitation (which affects tropical and equatorial areas), and it is a function of climatic hazards [17-19].

In this study, to determine geochemical processes contributing to water mineralization, major constituents and stable isotopes of GW from SS Moroccan L-D region were evaluated using chemical technics and AAS.

Experimental

Investigated zone

The investigated zone is L-D (Fig. 1), in SS Morocco (17°E - 11°E. 20°40′N - 28°48′N).

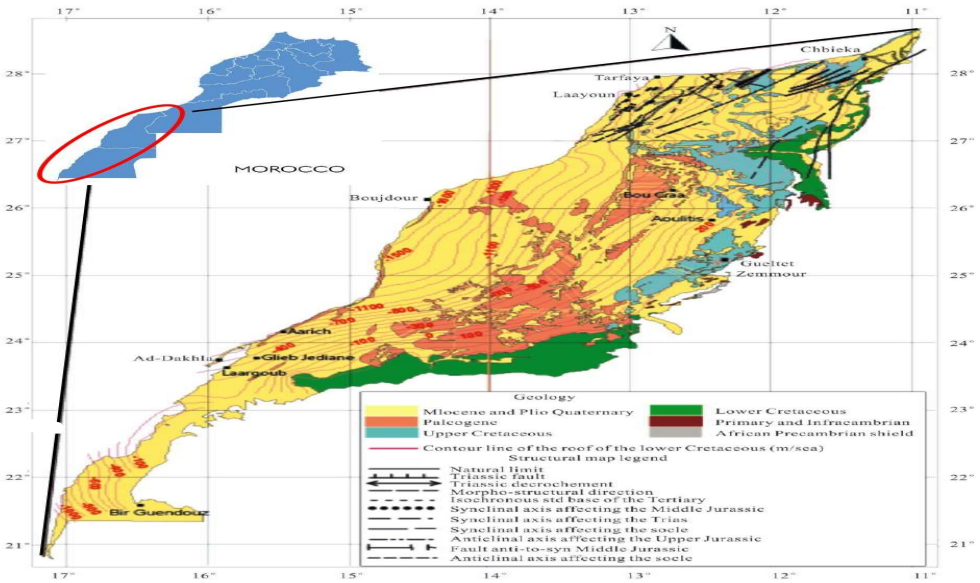

Figure 1: Geographical location of L-D, presenting the lower cretaceous rock roof and the structural basin [13, 23].

It is a sedimentary basin with an area of about 326.810 km^2, made up of tabular plains extending on the west by the Atlantic Ocean and on the southeast by the Zemmour fault, with widths ranging from 400 km to 400 m and heights from 0 to 400 m. These formations separate older African massifs such as Anti-Atlas and Mauritania series, and Tindouf basin. Thus, they have considerable GW resources that flow into a complex aquifer made up of deep waters. So, there are three different aquifers in this basin: Plio-Quaternary formations with alluvial aquifers (such as the water layer from Laayoune and Foum El Oued); Paleogene aquifer with Marly sands (they generally come across in depths ranging from 150 to 300 m); and Lower Cretaceous aquifer which is in sandstone. This is the largest Saharan basin, due to its area and lithology, which allow for a massive supply of GW.

Geological study

Tarfaya-Aaiun (Laâyoune) basin extends from Tarfaya to Ifni, along Moroccan Sahara [20]. Several authors have studied its geology, concluding that it consists of folded Precambrian and Paleozoic rocks covered by Mesozoic sediments of which thickness locally surpasses 12 km [21, 22]. The Plio-Quaternary aquifer is composed of marls from Upper Cretaceous and Miocene, and inferior sands, sandstone, dolomitic limestone, high sands and alluvia from Plio-Quaternary.

Along the Atlantic coast, Tarfaya-Dakhla washbasin resembles to Cretaceous and Neogene sediments dropped on Triassic-Jurassic syn-Atlantic bonds. Thus, Cretaceous marginal platforms rocks resemble to marine lagoon sediments with black shales rich in organic matter from Cenomanian-Turonian boundary. Paleocene-Eocene tinny sandy-marl sediments overlie Upper Cretaceous strata which, in turn, are covered by Miocene sequence, that thickens abruptly to the west [23].

Claystone, marl, siltstone and dolomitic limestone constitute Upper Albian to Lower Cenomanian sequence [24]. Deeper-water shale and limestone are found in Upper Cenomanian-Turonian and Coniacian layers, charted by the shallow water oyster shell couches from Santonian. Altogether, Palaeocene, Upper Cretaceous and Lower Cretaceous sediments are condensed by an erosional unconformity [20]. This erosion was produced between Santonian and Paleocene eras. Thin Eocene and Oligocene units are overlaid by a thicker Miocene layer that can reach a width of over 1 km [20].

Used materials and technics

All GW samples were taken from 30 wells (shallow and deep) in the year 2019. They were recovered and stored in polyethylene bottles, at 4 ºC. The analytical techniques employed are those previously made available by water analysis [25].

Physicochemical parameters (T, pH, EC and TDS) were obtained *in situ*, using a conductivity meter instrument (pH-meter PCE-PHD 1). Cationic ions (Ca^{2+}, Mg^{2+}, Na^{+} and K^{+}) Ct were determined by AAS (iCE-3000 AAS; Thermo Scientific), while anionic ions (HCO_3^- and Cl^-) Ct were determined by chemical dosage, employing HCl and silver nitrate (0.1 N). Additionally, NO_3^- and SO_4^{2-} ions were obtained using colorimetric methods, with a UV-vis spectrophotometer Cecil CE-7500 instrument. $\delta^{18}O$ and $\delta^{2}H$ were obtained by MS. Employing techniques suggested by [26] and [27], every example was analyzed thrice, to

obtain exact measures. Stable isotope analyses (^{18}O and ^{2}H) were performed using IRMS. With AQUAPREP automaton and CO_2 equilibration, ^{18}O analysis was performed using dual inlet method (0.05) error. ^{2}H analysis was made employing continuous flow method, with a Eurovector PYROH Elemental analyzer, by pyrolyzing water in Cr presence, under He flow (0.8 error). The obtained values are given in δ(‰), relative to V-SMOW international standard. Moreover, statistics were carried out by Aqua Chem 2014.2, which may exhibit qualified amounts of numerous ions in every studied GW sample.

Results and discussion

Table 1 presents results obtained from the analysis of physicochemical parameters for L-D area studied water. It is noteworthy that pH values of GW from the studied region ranged from 6.88 to 7.75, with an average of 7.34. This suggests a neutral nature of the investigated GW. EC and TDS values are significantly high, 3341.53 µs/cm and 2505.66 mg/L, respectively.

Table 1: Various physicochemical parameters results of L-D region water.

Wells	X	Y	T	pH	EC	TDS	HCO_3^-	Cl^-	SO_4^{2-}	NO_3	Ca^{2+}	Mg^{2+}	Na^+	K^+
	m	m	°C		µs/cm	mg/L	mg/L	mg/L	mg/L	mg/L	mg/L	mg/L	mg/L	mg/L
W1	757879	3036372	36	7.48	4700	3210	201.37	1303.14	1190.79	0	422.44	129.28	913.85	30.11
W2	738000	2963000	34.6	7.55	2880	2540	225.77	1175.00	1510.70	0	402.00	124.42	765.65	24.24
W3	701599	2947370	54.5	7.32	6390	4740	152.55	684.19	1908.43	0	724.65	69.98	487.18	17.20
W4	732675	2981680	40	7.33	3620	2470	189.16	959.63	744.24	0	349.50	61.24	618.44	20.72
W5	764800	2935500	30	6.88	3030	2070	360.02	787.70	371.31	0	301.43	100.12	465.78	18.77
W6	762450	2936500	30	7.00	2795	2120	360.02	816.41	381.40	0	333.47	40.34	448.76	19.94
W7	762200	2934400	30	7.00	2584	1960	317.30	744.80	353.06	0	209.76	87.84	459.80	17.99
W8	753597.7	2855142.5	29	6.90	6895	5230	353.92	2164.07	699.39	9.30	423.44	188.69	1310.43	17.20
W9	715200	2916800	27	7.40	6750	5900	976.30	1074.14	2200.48	2.48	942.48	269.73	665.78	72.34
W10	735165.3	2829710.6	29	6.93	1700	1400	475.96	400.94	165.55	0	134.07	59.29	307.84	10.17
W11	723200	2904034	40	7.34	5600	4820	353.92	2327.29	239.21	6.82	322.24	128.18	1460.32	51.22
W12	570380	2770285	22.1	7.22	4070	2780	139.74	709.71	1418.95	0	619.09	122.47	396.81	52.00
W13	562000	2767735	49	7.45	3550	2420	128.14	808.97	600.44	0.62	221.24	39.85	637.97	13.69
W14	596099.8	2833063.9	44	7.34	5010	4110	268.49	888.02	2378.69	0	733.56	48.60	691.46	19.16
W15	405433	2622099	36	7.34	2630	1790	207.47	744.80	254.11	0	227.65	35.72	489.89	17.60
W16	406340	2628134	33.5	7.75	2740	1870	164.75	798.33	249.30	0	157.11	30.25	574.75	19.16
W17	427599	2643318	38.4	7.55	2307	1750	201.37	758.98	198.38	0	134.27	25.03	580.73	13.69
W18	414890	2614006	28.3	7.21	2200	1500	256.28	572.87	266.11	0	224.45	47.63	359.79	8.99
W19	411263	2611042	32	7.35	2210	1910	274.59	544.16	260.35	0	218.04	44.35	339.79	12.90
W20	426224	2611569	36	7.42	2690	1830	183.06	629.59	717.29	0	343.08	52.49	439.80	18.11
W21	442014	2661785	35	7.73	2175	1650	176.96	687.38	95.11	0	105.21	36.94	370.83	17.20
W22	465000	2653100	35.5	7.29	2920	1990	170.86	758.98	220.00	0	150.30	37.91	505.67	12.90
W23	406426	2628734	36.5	7.74	2780	1900	164.75	716.09	227.21	0.62	87.37	14.58	486.70	12.90
W24	390220	2570860	32	7.75	5590	4820	109.84	1059.60	397.29	3.72	237.27	40.82	735.47	19.94
W25	341668	2429916	36	7.14	2690	1840	231.88	687.38	199.35	14.88	142.48	36.94	465.55	9.78
W26	547250	2641900	26	7.37	3320	2270	231.88	798.33	275.72	56.43	181.02	46.66	569.00	5.87
W27	671150	2670650	24	7.38	2170	1480	183.06	487.08	180.13	54.57	129.08	30.13	296.80	5.08
W28	648761	2654854	27.9	7.33	1610	1030	262.39	329.33	179.17	27.28	104.45	23.33	220.93	5.08
W29	644465	2642845	26	7.44	1290	850	231.88	200.65	147.95	24.80	90.94	18.47	134.03	3.91
W30	644598	2642784	26	7.33	1350	920	231.88	229.01	176.29	26.66	82.76	49.57	123.92	5.08

Ct of Ca^{2+} and Mg^{2+} varied from 82.76 to 942.48 mg/L and from 14.58 mg/L to 269.73 mg/L, with an average of 291.83 and 68.03 mg/L, respectively. In addition, Ct of Na^+ and K^+ varied from 123.92 to 1460.32 mg/L and from 3.91 to 72.34 mg/L, with an average of 290.47 and 15.033 mg/L, respectively. Table 1 shows that main anions in the studied zone alternated from 200.65 to 2327.29 mg/L, 95.11 to 2378.69 mg/L, 109.84 to 976.30 mg/L and 0 to 56.43 mg/L, for Cl^-, SO_4^{2-}, HCO_3^- and NO_3^- ions, respectively. In fact, NO_3^- levels in most wells were low, under the boundary value defined by Moroccan standard (50 mg/L), apart from wells W26

and W27, of which maxima values were 56.43 mg/L. NO_3^- presence in this GW is due to the activities performed there, such as fertilizers application on the farms, plants break down, discharge of human wastewater and domestic effluents [28]. On the other hand, it is seen that the main cations mean molar has the following order: $Na^+ > Ca^{2+} > Mg^{2+} > K^+$. Anions trend as follows: $Cl^- > SO_4^{2-} > HCO_3^- > NO_3^-$.

HG facies of the investigated water

To determine HG facies of the GW samples, Piper diagram was used, and Fig. 2 represents the obtained results.

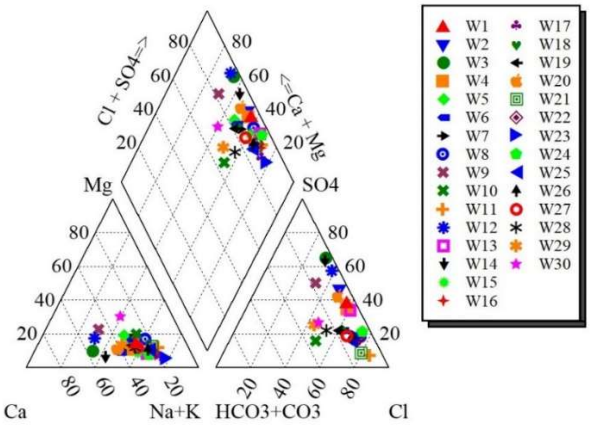

Figure 2: Representative piper graphs for the investigated GW categories.

GW samples have a dominant percentage of 86.66% Na-Cl, probably due to evaporates deposits, and a main value of 13.33% Ca-SO_4. In addition, the slight trend near facies of Ca-SO_4 is perhaps due to gypsum lens dissolution situated in marly formations of Miocene, or by schist in the south of the studied zone. This indicates and confirms that GW quality is affected by several parameters, such as chemistry, reservoir rocks geology and anthropogenic factors [29, 30].

HG procedures determination

It is known that water-rock interfaces play a significant role in GW quality modification. They are also beneficial for identifying GW sources. To explain various HG intricate actions for developing water chemistry, the relationship between presented ionic elements was studied using dispersion plots [31]. When the relationship is very adjacent to the right 1:1, the dependency grade is rectilinear between variables [32]. This investigation may tell the source of diverse waters, and the procedures that created their chemical composition [10, 33]. In addition, to determine occurred HG procedures, numerous graphical standards are often employed. Fig. 3 represents Ct of Cl *vs*. Ct of Na diagram for the studied waters.
This diagram is often employed to determine the procedure responsible for water salinity [34]. It is found that most samples are situated alongside NaCl halite solubility line (i.e., where the Na/Cl molar quotient = 1), which is related to the marine spray dissolved by rainwater (sea salt), or to evaporites modification [35]. In addition, the correlation factor between chemical constituents (Na^+ and Cl) in the investigated GW was very high (R = 0.98). This finding indicates that their

correlations are quite robust, since they have an identical source. Indeed, it is noticed that the source has a dry location, with high-speed evapotranspiration, which causes the formation of salt deposits that are splashed into GW [36].

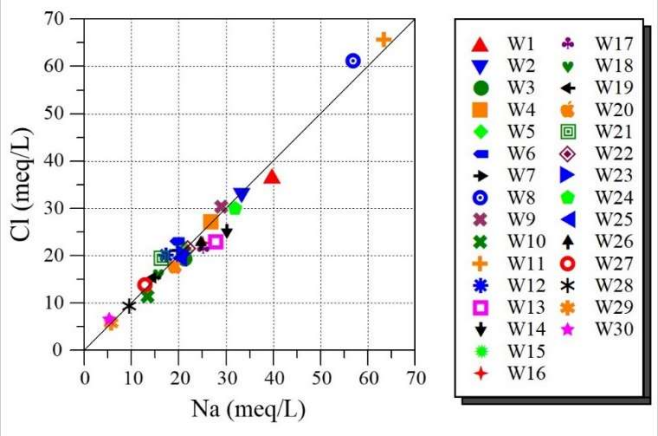

Figure 3: Ct of Cl *vs*. Ct of Na diagram for the tested samples.

This diagram is often employed to determine the procedure responsible for water salinity [34]. It is found that most samples are situated alongside NaCl halite solubility line (i.e., where the Na/Cl molar quotient = 1), which is related to the marine spray dissolved by rainwater (sea salt), or to evaporites modification [35]. In addition, the correlation factor between chemical constituents (Na^+ and Cl) in the investigated GW was very high (R = 0.98). This finding indicates that their correlations are quite robust, since they have an identical source. Indeed, it is noticed that the source has a dry location, with high-speed evapotranspiration, which causes the formation of salt deposits that are splashed into the GW [36].

Source of Ca^{2+}, Mg^{2+}, HCO_3^- and SO_4^{2-} ions

Fig. 4 represents the plot of SO_4^{2-} + HCO_3^- *vs*. Ca^{2+} + Mg^{2+} ions.

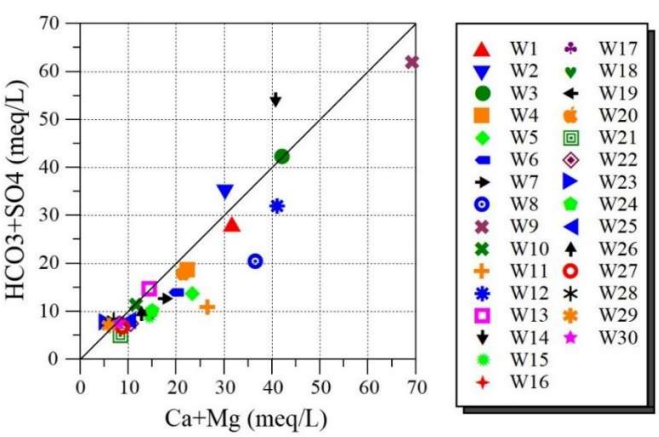

Figure 4: Representation plot of Ca^{2+} + Mg^{2+} vs. SO_4^{2-} + HCO_3^- ions.

It is seen that GW samples are dispersed on line 1:1 (least mineralized) and beyond. In addition, samples adjacent to 1:1 display that calcite, dolomite and gypsum dissolution is the main mechanism in the system [37].

However, in CO_3^{2-} media, simultaneous Ca^{2+} ions enhancement and Mg^{2+} ions diminution are principally due to interaction phenomena between rocks and water, such as dolomitization, dissolution and precipitation [38].
On the other hand, Fig. 5 is the graphic representation of Ca^{2+} vs. Mg^{2+} ions.

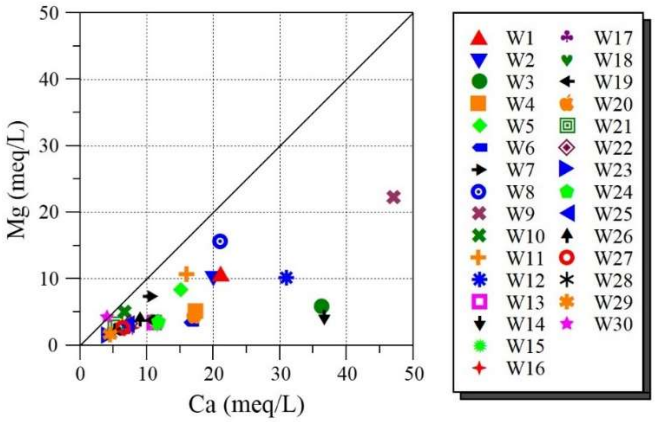

Figure 5: Representation plot of Ca^{2+} vs. Mg^{2+}ions.

It is seen that some of the studied GW points have a Mg^{2+}/Ca^{2+} ratio different from 1:1 line. This finding means that Ct of Ca^{2+} is higher than that of Mg^{2+} ions. Ca^{2+} source mainly comes from gypsum dissolution. It is known that dolomite dissolution results in a 1:1 relationship between alkalinity and Ca^{2+} + Mg^{2+} ions. Indeed, Fig. 6 represents the variation in Ca^{2+} + Mg^{2+} *vs*. HCO^{3-} ions and Ca^{2+} vs. HCO^{3-} ions.

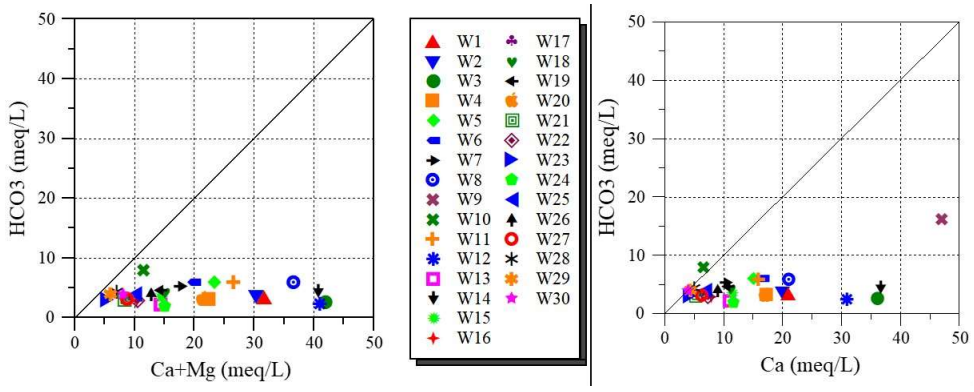

Figure 6: Representation plot of Ca^{2+} and Ca^{2+} + Mg^{2+} ions as a function of HCO^{3-} ions.

It was noticed that the relationship between alkalinity and Ca^{2+} + Mg^{2+} ions is weak. This finding shows that dolomite dissolution was not the principal source of Ca^{2+} and Mg^{2+} ions in the studied GW area. Moreover, the relationship between alkalinity and Ca^{2+} ions is quite weak, indicating HCO^{3-} ion reduction.
Nevertheless, Fig. 7 represents the plot of Ca^{2+} *vs*. SO_4^{2-} ions. It is seen that the bulk of investigated GW is dispersed nearby the gypsum dissolution line. This confirms the source of Ca and SO_4 ions dissolution (gypsum). Additionally, the obtained association between Ca and SO_4 ions proposes the discharge of gypsum and anhydrite, when water runs underground.

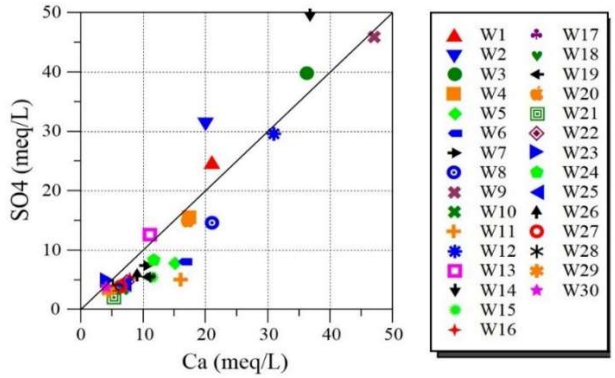

Figure 7: Representation plot of Ca^{2+} ions *vs*. SO_4^{2-} ions.

For more details, Fig. 8 shows the representation plot of Na^+ ions *vs*. HCO_3^- ions. A poor correlation between alkalinity and Na^+ ions was obtained. This result suggests that Na_2CO_3 dissolution is not significant in the investigated area.

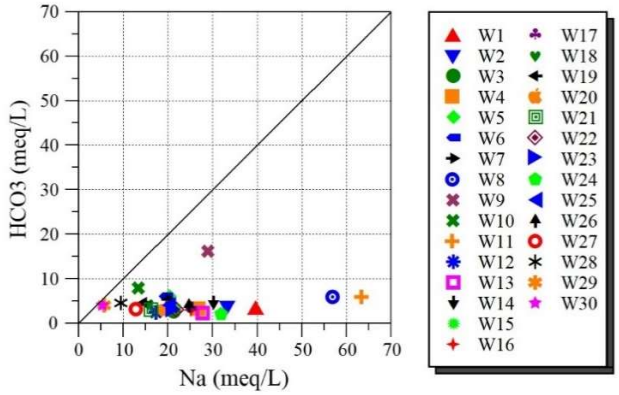

Figure 8: Representation plot of Na^+ *vs*. HCO_3^- ions.

In fact, the studied SS zone is in the arid region, which offers an advantageous circumstance for evaporation and condensation. Due to evaporation, Cl^- ions in GW from arid zones is high, which reflects its mineralization degree. Additionally, Fig. 9 shows the plot of TDS *vs*. Cl^- ions. It is seen that Ct of Cl^- rises with TDS growth, indicating that the investigated GW was affected by the evaporation phenomenon.

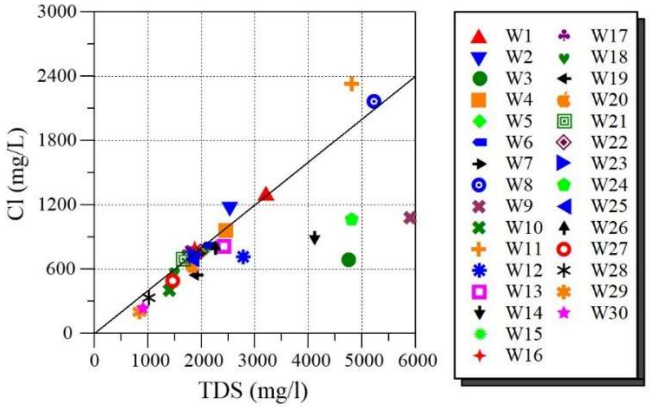

Figure 9: Representation plot of TDS vs. Cl^- ions.

Mineral dissolution/precipitation: Gibbs diagram

It is known that the interaction between GW and aquifer minerals has an essential role in water quality, which is also suitable for determining its source [39]. Gibbs [40] proposed a diagram where cations (Fig. 10a)) [(Na + K)/(Na + K + Ca)] and anions [Cl/(Cl + HCO_3)] proportion (Fig. 10b)) is expressed in the relationship with TDS.

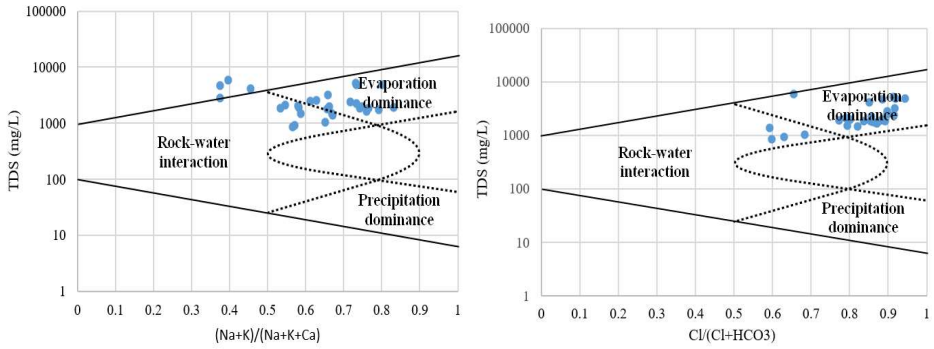

Figure 10: Gibbs plot of **(a)** cations and **(b)** anions for investigated GW from Moroccan L-D area.

Fig. 10a and b represent obtained Gibbs plot for investigated GW from Moroccan L-D zone. It is seen that most of the studied samples were found at the evaporation area, where its effect foremost occurs in the investigated GW region. Therefore, it is concluded that the evaporative dissolution procedure governs GW chemistry in this area. In addition, it is noticed that most tester walls are in the evaporation area, which may be due to climatic circumstances (arid weather).

SI at chemical stability

According to literature, fresh-water quality and exchanges of water with soil and rocks through percolation and packing in aquifers play a very important role in the determination of GW chemistry [40]. Indeed, SI are generally employed to define the trend of water towards precipitation or salt dissolution. Fig. 11 represents SI evolution of the investigated GW.

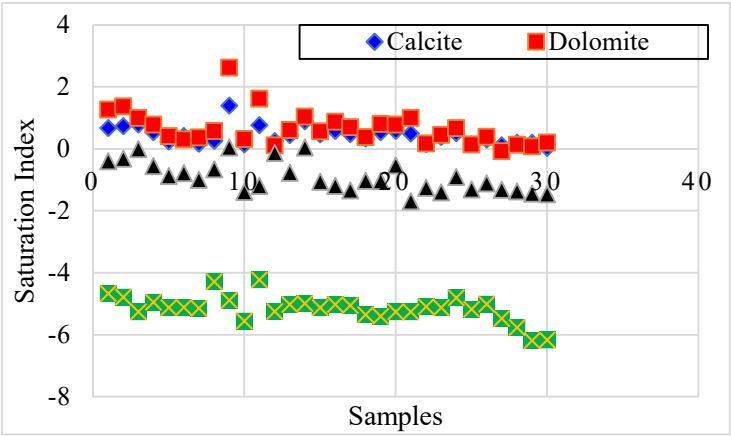

Figure 11: SI variation of the investigated GW.

According to geochemical modeling results on GW development, there is an important relation between SO_4^{2-} ions and SI of carefully chosen minerals. These findings reveal that CO_3^{2-} precipitation is intensely influenced by evaporative mineral dissolution.

Isotope results

The investigation of stable isotopes from water molecules was widely employed for studying GW. They offer more data on the water source and on how the GW is renewed. They also define small and durable climatic changes, and allow the quantitative valuation of mixing and other procedures, such as those reported by [42, 43]. Indeed, GW salinity origin can be found by stable isotopes configurations [44]. They are equivalent to that of GMWL: δ^2H (‰) = 8*$\delta^{18}O$ (‰) + 10 [45]. [46] revealed that this relation is caused by isotopic water particles fraction through evaporation and condensation phenomena in hydrological cycle. Table 2 shows isotopic analyses of waters from the studied L-D region.

It is seen that O and δ^2H values of the thirty studied GW testers changed from -6.96 to -8.93‰, and from -51.5 to -65.56‰, for $\delta^{18}O$ and δ^2H isotopes, respectively. These ranges describe an Atlantic source of precipitation. In addition, their findings are almost like those determined by other researchers [23].

Indeed, evaporation usually occurs through the surface runoff in lakes and reservoirs [47]. Thus, the effect of isotopic conversion procedure can modify GW isotopic structure, which must also be taken into account [43]. Moreover, atmospheric T is a main factor that controls isotopic composition and $\delta D/\delta^{18}O$ relation of water [48].

Table 2: Isotopic analysis results of investigated samples.

Wells	T °C	pH	EC µs/cm	TDS mg/L	Depth m	^{18}O‰	^{2}H‰
W1	36	7.48	4700	3210	450	-8.78	-64.1
W2	34.6	7.55	2880	2540	629	-8.63	-62.55
W3	54.5	7.32	6390	4740	920	-8.93	-63.55
W4	40	7.33	3620	2470	650	-8.55	-63.05
W5	30	6.88	3030	2070	552	-8.78	-63.9
W6	30	7	2795	2120	452	-8.77	-65
W7	30	7	2584	1960	497	-8.76	-65.56
W8	29	6.9	6895	5230	450	-7.31	-57.64
W9	27	7.4	6750	5900	390	-8.82	-60.1
W10	29	6.93	1700	1400	260	-8.23	-58.13
W11	40	7.34	5600	4820	-	-	-
W12	22.1	7.22	4070	2780	145	-8.57	-63.6
W13	49	7.45	3550	2420	900	-8.32	-60.9
W14	44	7.34	5010	4110	881	-8.7	-63.25
W15	36	7.34	2630	1790	510	-8.32	-63.22
W16	33.5	7.75	2740	1870	470	-8.26	-63.31
W17	38.4	7.55	2307	1750	543	-8.37	-62.23
W18	28.3	7.21	2200	1500	315	-8.39	-62.67
W19	32	7.35	2210	1910	415	-8.42	-63.13
W20	36	7.42	2690	1830	490	-8.48	-62.36
W21	35	7.73	2175	1650	720	-8.65	-60.65
W22	35.5	7.29	2920	1990	525	-8.27	-63
W23	36.5	7.74	2780	1900	530	-8.43	-62.25
W24	32	7.75	5590	4820	350	-8.59	-62.65
W25	36	7.14	2690	1840	450	-6.96	-51.5
W26	26	7.37	3320	2270	180	-7.73	-58.25
W27	24	7.38	2170	1480	140	-8.4	-62.55
W28	27.9	7.33	1610	1030	175	-8.63	-62.75
W29	26	7.44	1290	850	156	-8.66	-62.85
W30	26	7.33	1350	920	165	-8.62	-63.45

Fig. 12 represents the diagram of isotopic composition (δ^2H, $\delta^{18}O$) *vs*. LMWL and GMWL.

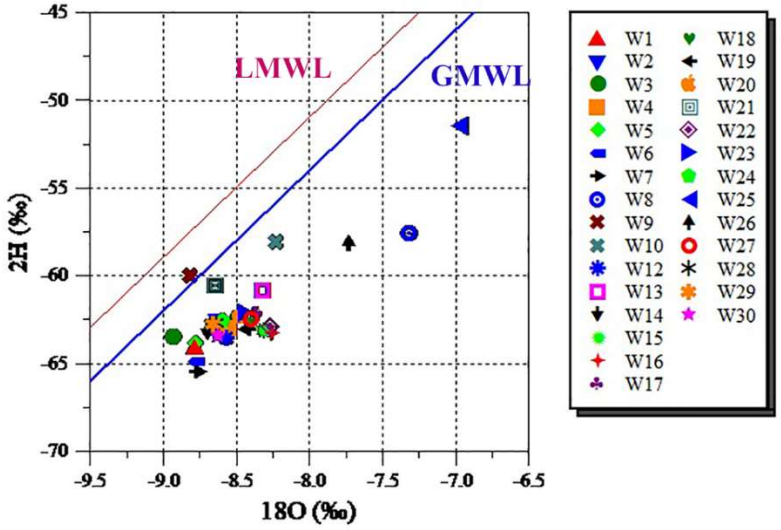

Figure 12: Relation of d^2H and $d^{18}O$ to LMWL [49] and GMWL [45] for investigated GW.

Thus, to assess the determined values for both meteoric water lines, it is seen that the complete points of tested GW are strategized to the right, describing a trend with an inclination of 5.35, and reproducing an evaporation incline between 4 and 6 in arid and semi-arid zones [43, 50, 51]. These results suggest either evaporation of raindrops before hitting the ground [52], or overdue infiltration of precipitation, and a mixture of meteoric water with evaporated rain, in some limited samples [23].

In its turn, determining altitudes and recharge zones in the origin is very important for estimating GW assets. Thus, the stable isotope rank is employed to define fresh-water elevations. In addition, wastewater isotopic sign is frequently used *vs*. soil T, where the seepage follows [53]. For this, the probable relation between $\delta^{18}O$ isotopic quotient and water infiltration altitude was defined. Fig. 13 represents $\delta^{18}O$ values and elevations of various investigated GW. Herein, a line drawn to give local altitude isotopic slope was obtained at -0.52‰ per 100 m.

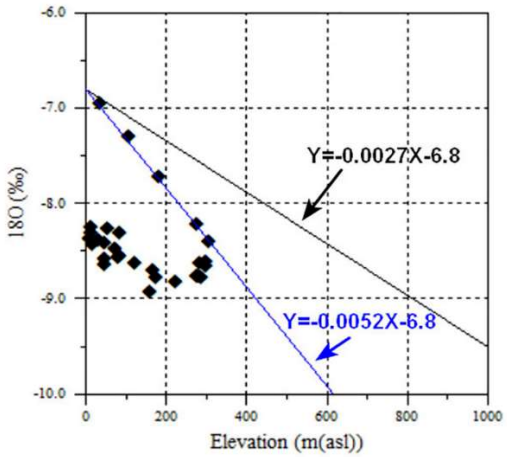

Figure 13: Altitude -$\delta^{18}O$ plot for investigated GW.

Thus, the obtained values are dissimilar from those presented in literature. In fact, on Morocco rule, the local altitude isotopic slope was about -0.27‰ per 100 m altitude [54]. So, water should be recharged at altitudes that do not exceed 300 m above sea level. However, variations in isotopic structures between the aquifer and precipitation (which have been employed to define the slope) cannot be assigned to altitude, and may have been caused by soil T.

Conclusion

Combined HG and stable isotopes ($\delta^{18}O$, $\delta^{2}H$) practical approach in this investigation led to a good comprehension of the function of GW system in the studied L-D area, where mineralization procedure caused a significant modification in composition. Obtained HG parameters showed that abundant cations and anions followed the trend: $Na^+ > Ca^{2+} > Mg^{2+} > K^+$ and $Cl^- > SO_4^{2-} > HCO_3^- > NO_3^-$, respectively. In addition, two dominant HG facies were founded for GW of the studied zone: Na-Cl and Ca-SO_4, with 86.66% of the former. It was also revealed that the main procedures in water mineralization are evaporation and minerals dissolution phenomena. Moreover, stable isotope data indicated an important origin of meteoric water recharge linked to a predominance of evaporation in the increase in salt Ct. Finally, it was found that waters are recharged at altitudes not higher than 300 m.

Authors' contributions

K. Mizeb: collected data; conceived and designed analyses; performed analyses. **M. Doubi:** conceived and designed analyses; collected data; conceived and designed analyses; wrote the paper. **M. Ghalit:** collected data; contributed with data or analyses tools. **M. El Kanti:** conceived and designed analyses; collected data; contributed with data or analyses tools. **H. Erramli:** conceived and designed analyses; contributed with analyses tools; conceived and designed analyses. **R. Touir:** conceived and designed analyses; collected data; contributed with data or analyses tools; conceived and designed analyses; wrote the paper.

Abbreviations

AAS: atomic absorption spectroscopy
Ca-SO_4: calcium sulfate
CO_3^{2-}: carbonate
Ct: concentration
EC: electrical conductivity
GMWL: global meteoric water line
GW: groundwater
HCO_3^-: hydrogencarbonate
HG: hydrogeochemical
IRMS: isoprime precision isotope ratio mass spectrometer
L-D: Laayoune-Dakhla
LMWL: local meteoric water line
MS: mass spectrometry

MW: makeup water (water added to compensate for losses, especially those caused by evaporation)
Na_2CO_3: sodium carbonate
Na-Cl: sodium chloride
NO_3^-: nitrate
SI: saturation index
SO_4^{2-} : sulphate
SS: southern Sahara
T: temperature
TDS: total dissolved solids
UV-vis: visible ultra-violet
V-SMOW: Vienna-standard mean ocean water

Symbols definition
‰: per mile
δ^2H: deuterium
$\delta^{18}O$: oxygen-18

References

1. Liu J, Gao Z, Wang M et al. Hydrochemical characteristics and possible controls in the groundwater of the Yarlung Zangbo River Valley, China. Environm Earth Sci. 2019;78:1-11. https://doi.org/10.1007/s12665-019-8101-y
2. Doubi M, Darif H, Koulou A et al. Evaluation of Souss-Massa Daraa Region Irrigation Groundwater Hydrogeochemical Characteristics and Quality: A Multivariate Statistical Approach. Port Electrochim Acta. 2022;40:425-440. https://doi.org/10.4152/pea.202240060
3. Richards LA, Fox BG, Bowes MJ et al. A systematic approach to understand hydrogeochemical dynamics in large river systems: Development and application to the River Ganges (Ganga) in India. Water Res. 2022; 54:211-224. https://doi.org/10.1016/j.watres.2022.118054
4. Boelee E, Geerling G, van der Zaan B et al. Water and health: From environmental pressures to integrated responses. Acta Tropica. 2019;193: 217-226. https://doi.org/10.1016/j.actatropica.2019.03.011
5. Es-sousy M, Gharibi E, Ghalit M et al. Hydrochemical quality of the Angads plain groundwater (Eastern Morocco). Arab J Geosci (CAJG-1). Tunisia Springer International Publishing. 2019;24:99-102. https://doi.org/10.1007/978-3-030-01572-5_24
6. Su F, Li P, Fida M. Dominant factors influencing changes in the water quantity and quality in the Dianshi Reservoir, East China. Human Ecolog Risk Assess: Int J. 2022;28:387-407. https://doi.org/10.1080/10807039.2022.2053355
7. Zhang B, Zhao D, Zhou P et al. Hydrochemical characteristics of groundwater and dominant water–rock interactions in the Delingha Area, Qaidam Basin, Northwest China. Water. 2020;12:83-96. https://doi.org/10.3390/w12030836
8. Gharibi E, Ghalit M, Taupin JD et al. Effect of saltwater intrusion due to over-exploitation and earthquakes on mineralization processes of spring waters over the Massif Bokkoya (central Rif, Morocco). J Water Suppl: Res Technol—AQUA. 2017;66:279-286. https://doi.org/10.2166/aqua.2017.112

9. Romanova A, Porowski A, Zielski T et al. Origin and evolution of chemical composition of mineral waters of Szczawno-Zdrój inferred from long-term variation of ionic ratios, Sudetes Mts. (SW Poland). Environ Earth Sci. 2021;80: 374-390. https://doi.org/10.1007/s12665-021-09643-1
10. Bouaissa M, Gharibi E, Ghalit M et al. Identifying the origin of groundwater salinization in the Bokoya massif (central Rif, northern Morocco) using hydrogeochemical and isotopic tools. Groundwat Sustain Devel. 2021;14: 76-89. https://doi.org/10.1016/j.gsd.2021.100646
11. Elmeknassi M, Bouchaou L, El Mandour A et al. Multiple stable isotopes and geochemical approaches to elucidate groundwater salinity and contamination in the critical coastal zone: A case from the Bou-areg and Gareb aquifers (North-Eastern Morocco). Environ Pollut. 2022;300:118942. https://doi.org/10.1016/j.envpol.2022.118942
12. Bouteldjaoui F, Bessenasse M, Taupin JD et al. Mineralization mechanisms of groundwater in a semi-arid area in Algeria: statistical and hydrogeochemical approaches. J Water Sup: Res Technol-Aqua. 2020; 69:173-183. https://doi.org/10.2166/aqua.2019.116
13. Mizeb K, Doubi M, Ghalit M et al. Quality assessment of groundwater in the region of Laayoune-Dakhla (southern Sahara Morocco) for drinking and irrigation purposes. Moroc J Chem. 2022;10:10-3. https://doi.org/10.48317/IMIST.PRSM/morjchem-v10i3.33070
14. Jung H, Koh DC, Kim YS et al. Stable isotopes of water and nitrate for the identification of groundwater flowpaths: A review. Water. 2020;12:138. https://doi.org/10.3390/w12010138
15. Doubi M, Nimour A, Dermaj A et al. Physicochemical Analysis of Ground Water Quality, Hydrochemical Characterization of the Doukkala plain, Morocco. Orient J Chem. 2021;33:2632-2638. http://dx.doi.org/10.13005/ojc/370213
16. Lone SA, Jeelani G, Padhya V et al. Identifying and estimating the sources of river flow in the cold arid desert environment of Upper Indus River Basin (UIRB), western Himalayas. Sci Total Environ. 2022;832:154964. https://doi.org/10.1016/j.scitotenv.2022.154964
17. McGill LM, Brooks JR et al. Spatiotemporal dynamics of water sources in a mountain river basin inferred through δ2H and δ18O of water. Hydrologic Proc. 2021;35:14063. https://doi.org/10.1002/hyp.14063
18. Ghalit M, Bouaissa M, Gharibi E et al. Hydrogeochemical Characteristics and Isotopic Tools Used to Identify the Mineralization Processes of Bottled Mineral Water in Morocco. Geosciences. 2023;13:38. https://doi.org/10.3390/geosciences13020038
19. Zhao P, Guo ZS, She DL et al. (Spatial distribution of the oxygen-18 in precipitation in China based on a new empirical model. J Mount Sci. 2019; 16:2605-2614. https://doi.org/10.1007/s11629-019-5514-8
20. Davison I. Central Atlantic margin basins of North West Africa: geology and hydrocarbon potential (Morocco to Guinea). J Afri Earth Sci. 2005; 43:254-274. https://doi.org/10.1016/j.jafrearsci.2005.07.018
21. Michard A. 1976. Eléments de Géologie Marocaine.
22. Kolonic S, Sinninghe DJ, Böttcher S et al. Geochemical characterization of cenomanian/turonian black shales from the tarfaya basin (sw morocco) relationships between palaeoenvironmental conditions and early sulphurization of sedimentary organic matter. J Petrol Geol. 2002;25:325-350. https://doi.org/10.1111/j.1747-5457.2002.tb00012.x

23. Edoulati N, Boutaleb S, Bettar I et al. Contributions of chemical and isotopic tools for understanding the groundwater modes recharge and flow in the lower Cretaceous aquifer in the Moroccan Sahara. J Water Res Prot. 2013;5:183-199. https://doi.org/10.4236/jwarp.2013.52020
24. Wiedmann J, Butt A, Einsele G. Cretaceous stratigraphy, environment, and subsidence history at the Moroccan continental margin. In Geology of the northwest African continental margin. 1982;366-395. Springer Berlin Heidelberg. https://doi.org/10.1007/978-3-642-68409-8_15
25. Rodier J, Legube B, Merlet N. L'Analyse de l'eau (Water analysis). 9e édition.
26. Epstein S, Mayeda T. Variation of O18 content of waters from natural sources. Geochim Cosmochim Acta. 1953;4:213-224. https://doi.org/10.1016/0016-7037(53)90051-9
27. Friedman I. Deuterium content of natural waters and other substances. Geochim Cosmochim Acta. 1953;4:89-103. https://doi.org/10.1016/0016-7037(53)90066-0
28. Doubi M, Nimour A, Aouine Y et al. Assessment of physico-chemical quality of groundwater in the plain of Bahira (Bassin Oum Errabia). Ind J Environ Prot. 2021;41:347-353.
29. Emenike CP, Tenebe IT, Omole DO et al. Accessing safe drinking water in sub-Saharan Africa: Issues and challenges in South–West Nigeria. Sustain Cities Soc. 2017;30:263-272. https://doi.org/10.1016/j.scs.2017.01.005
30. Ben-aazza S, Hadfi A, Mohareb S et al. Geochemical characterization and thermodynamic study of water scaling phenomenon at Tiznit region in Southern Morocco. Groundwat Sustain Develop. 2020;11:100379. https://doi.org/10.1016/j.gsd.2020.100379
31. Sangadi P, Kuppan C, Ravinathan P. Effect of hydro-geochemical processes and saltwater intrusion on groundwater quality and irrigational suitability assessed by geo-statistical techniques in coastal region of eastern Andhra Pradesh, India. Mar Pollut Bull. 2022;175:113390. https://doi.org/10.1016/j.marpolbul.2022.113390
32. Wu J, Li P, Wang D et al. Statistical and multivariate statistical techniques to trace the sources and affecting factors of groundwater pollution in a rapidly growing city on the Chinese Loess Plateau. Human Ecolog Risk Assess: Int J. 2020;26:1603-1621. https://doi.org/10.1080/10807039.2019.1594156
33. Iyakare JD, Taupin JD, Hitimana CN. et al. Hydrochemical study of bottled water in Rwanda and relationship with their origin. Water Supply. 2022; 22:1155-1167. https://doi.org/10.2166/ws.2021.211
34. Najib S, Fadili A, Mehdi K et al. Contribution of hydrochemical and geoelectrical approaches to investigate salinization process and seawater intrusion in the coastal aquifers of Chaouia, Morocco. J Contam Hydrol. 2017;198:24-36. https://doi.org/10.1016/j.jconhyd.2017.01.003
35. Khan F, Krishnaraj S, Raja P et al. Impact of hydrogeochemical processes and its evolution in controlling groundwater chemistry along the east coast of Tamil Nadu and Puducherry, India. Environ Sci Pollut Res. 2021;28:18567-18588. https://doi.org/10.1007/s11356-020-10912-y
36. Bali KM, Eltarabily MG, Berndtsson R et al. Nutrient and salinity management for spinach production under sprinkler irrigation in the low desert region of California. Irrig Sci. 2021;39:735-749. https://doi.org/10.1007/s00271-021-00740-4

37. Xiao Y, Shao J, Cui Y et al. Groundwater circulation and hydrogeochemical evolution in Nomhon of Qaidam Basin, northwest China. J Earth Syst Sci. 2017;126:1-16. https://doi.org/10.1007/s12040-017-0800-8
38. Yu Y, Song X, Zhang Y et al. Assessment of water quality using chemometrics and multivariate statistics: a case study in chaobai river replenished by reclaimed water, North China. Water. 2020;12:2551. https://doi.org/10.3390/w12092551
39. Bozdağ A, Göçmez G. Evaluation of groundwater quality in the Cihanbeyli basin, Konya, Central Anatolia, Turkey. Environ Earth Sci. 2013;69:921-937. https://doi.org/10.1007/s12665-012-1977-4
40. Gibbs RJ Mechanisms controlling world water chemistry. Science. 1970;170:1088-1090. https://doi.org/10.1126/science.170.3962.1088
41. Keesari T, Roy A, Mohokar H et al. Characterization of mechanisms and processes controlling groundwater recharge and its quality in drought-prone region of Central India (Buldhana, Maharashtra) using isotope hydrochemical and end-member mixing modeling. Nat Resour Res. 2020; 29:1951-1973. https://doi.org/10.1007/s11053-019-09550-0
42. Gat JR. The isotopes of hydrogen and oxygen in precipitation. In Handbook of environmental isotope geochemistry. Vol. 1.
43. Clark ID, Fritz P. Environmental isotopes in hydrogeology. CRC press. 2013;342. https://doi.org/10.1201/9781482242911
44. Bahir M, Ouhamdouch S, Ouazar D. An assessment of the changes in the behavior of the groundwater resources in arid environment with global warming in Morocco. Groundwat Sustain Develop. 2021;12:100541. https://doi.org/10.1016/j.gsd.2020.100541
45. Craig H. Isotopic variations in meteoric waters. Science. 1961;133:1702-1703. http://dx.doi.org/10.1126/science.133.3465.1702
46. Friedman I, Redfield AC, Schoen B et al. The variation of the deuterium content of natural waters in the hydrologic cycle. Rev Geophys. 1964;2: 177-224. https://doi.org/10.1029/RG002i001p00177
47. Clark ID, Jautzy JJ. Environmental Isotope Tracers. State Sci Pract. 15. CRC press. 1997 eBook ISBN:9780080929156.
48. Li Y, An W, Pang H et al. Variations of stable isotopic composition in atmospheric water vapor and their controlling factors—a 6-year continuous sampling study in Nanjing, eastern China. J Geophys Res: Atmosph. 2020;125:e2019JD031697. https://doi.org/10.1029/2019JD031697
49. Ouda B, El Hamdaoui A, Ibn Majah M. Isotopic composition of precipitation at three Moroccan stations influenced by oceanic and Mediterranean air masses. Isotopic composition of precipitation in the Mediterranean Basin in relation to air circulation patterns and climate. 2005; 125-140.
50. Abderamane H, Razack M, Vassolo S. Hydrogeochemical and isotopic characterization of the groundwater in the Chari-Baguirmi depression, Republic of Chad. Environ Earth Sci. 2013;69:2337-2350. https://doi.org/10.1007/s12665-012-2063-7
51. Ahmed M, Chen Y, Khalil MM. Isotopic composition of groundwater resources in arid environments. J Hydrol. 2022;609:127773. https://doi.org/10.1016/j.jhydrol.2022.127773

52. Sun C, Chen W, Chen Y et al. Stable isotopes of atmospheric precipitation and its environmental drivers in the Eastern Chinese Loess Plateau, China. J Hydrol. 2020;581:124404. https://doi.org/10.1016/j.jhydrol.2019.124404
53. Azioli A, Cervi F, Doveri M et al. Estimating the isotopic altitude gradient for hydrogeological studies in mountainous areas: Are the low-yield springs suitable? Insights from the northern Apennines of Italy. Water. 2019; 11:1764. https://doi.org/10.3390/w11091764
54. Miche H, Saracco G, Mayer A et al. Hydrochemical constraints between the karst Tabular Middle Atlas Causses and the Saïs basin (Morocco): implications of groundwater circulation. Hydrogeology J. 2018;26:71-87. https://doi.org/10.1007/s10040-017-1675-0